HHS Public Access

Author manuscript

*IEEE J Sel Top Quantum Electron*. Author manuscript; available in PMC 2022 July 01.

Published in final edited form as:

*IEEE J Sel Top Quantum Electron*. 2021 ; 27(4): . doi:10.1109/jstqe.2020.3024014.

# Photodynamic Priming Modulates Endothelial Cell-Cell Junction Phenotype for Light-activated Remote Control of Drug Delivery

**Collin T. Inglut**
Fischell Department of Bioengineering, University of Maryland, College Park, MD 20742, USA

**Kelsey M. Gray**
Fischell Department of Bioengineering, University of Maryland, College Park, MD 20742, USA

**Shruti Vig**
Fischell Department of Bioengineering, University of Maryland, College Park, MD 20742, USA

**Jae W. Jung**
Fischell Department of Bioengineering, University of Maryland, College Park, MD 20742, USA

**Jillian Stabile**
Fischell Department of Bioengineering, University of Maryland, College Park, MD 20742, USA

**Yuji Zhang**
Marlene and Stewart Greenebaum Comprehensive Cancer Center, University of Maryland, Baltimore, MD 21201, USA

Department of Epidemiology and Public Health, University of Maryland, Baltimore, MD 21201, USA.

**Kimberly M. Stroka**
Fischell Department of Bioengineering, University of Maryland, College Park, MD 20742, USA

Biophysics Program, University of Maryland, College Park, MD 20742, USA.

Center for Stem Cell Biology and Regenerative Medicine, University of Maryland, Baltimore, MD 21201, USA.

Marlene and Stewart Greenebaum Comprehensive Cancer Center, University of Maryland, Baltimore, MD 21201, USA

**Huang-Chiao Huang**
Fischell Department of Bioengineering, University of Maryland, College Park, MD 20742, USA

Marlene and Stewart Greenebaum Comprehensive Cancer Center, University of Maryland, Baltimore, MD 21201, USA

## Abstract



corresponding author: 301-405-6961; hchuang@umd.edu.

The blood-brain barrier (BBB) remains a major obstacle for drug delivery to the central nervous system. In particular, the tight and adherens junctions that join the brain capillary endothelial cells limit the diffusion of various molecules from the bloodstream into the brain. Photodynamic priming (PDP) is a non-cytotoxic modality that involves light activation of photosensitizers to photochemically modulate nearby molecules without killing the cells. Here we investigate the effects of sub-lethal photochemistry on junction phenotype (i.e., continuous, punctate, or perpendicular), as well as the BBB permeability in a transwell model of human brain microvascular endothelial cells (HBMECs). We showed that PDP decreases the continuous junction architecture by ~20%, increases the perpendicular junction architecture by ~40%, and has minimal impact on cell morphology in HBMECs. Furthermore, transwell permeability assay revealed that PDP improves the HBMEC permeability to dextran or nanoliposomes by up to 30-fold for 6–9 days. These results suggest that PDP could safely reverse the mature brain endothelial junctions without killing the HBMECs. This study not only emphasizes the critical roles of PDP in the modulation junction phenotype, but also highlights the opportunity to further develop PDP-based combinations that opens the cerebrum endothelium for enhanced drug transporter across the BBB.

**Index Terms—**

Benzoporphyrin derivatives; blood-brain barrier; light-controlled drug release; photochemistry; photodynamic priming

## I. Introduction

The brain is one of the most vascularized organs in the body. Despite differences in vessel architecture, diffusion of large or small compounds from the bloodstream into the brain are particularly challenging due to the intact blood-brain barrier (BBB). This specialized neurovascular unit, composed of endothelial cells, neural cells (e.g., astrocytes, pericytes, neurons) and basement membrane, regulates brain homeostasis and protects the central nervous system [1]-[3]. The cell-to-cell junctions that join the brain endothelial cells are composed of a wide variety of components, such as vascular endothelial-cadherin (VE-cadherin) adherens junction protein, zonula occludens (ZO) scaffold proteins, and claudin-5 tight junction protein. The tight junction transmembrane complexes located on the apical region of endothelial cells prevent the transport of hydrophilic, highly charged, and/or large (>400 Da) molecules [4]. In addition, astrocytes and pericytes secret growth factors and morphogens (e.g., cyclic AMP) to further enhance the formation and integrity of the junction network [5], [6]. The endothelial cell-cell junction at the BBB is one of the key factors that limit drug transport to the brain [7], [8]. Despite being the subject of studies for several decades, selective opening of the BBB junction network at the desired site without killing the brain endothelial cells remains a challenging task in the clinic.

A number of strategies have been developed to disrupt the tight junction network of the BBB, including the infusion of hyperosmolar solutions, biochemical disruption, focused ultrasound, and electromagnetic radiation [9]. Nevertheless, these methods are not yet universally available in the clinic due to a number of limitations, such as low efficiency,

invasiveness, lack of selectivity, or adverse events [9]-[12]. For example, clinical BBB opening with hypertonic solutions (e.g., arabinose, mannitol) lacks regional specificity and can induce a pronounced fluid shift [13], [14]. Existing site-specific methods (e.g., focused ultrasound [9], [15], [16] thermal therapy [17], [18], and radiation [19], [20]) can enhance drug delivery across the BBB but are often associated with increased risk of edema, hemorrhage, inflammation, or neurotoxicity. As a result, there is a clear need for a method that can dissociate the endothelial tight junction while sparing the endothelial cells.

Photodynamic therapy is a photochemistry-based treatment modality that involves the light activation of non-toxic photosensitizers or fluorescent dyes. High optical energy (e.g., 80–300 J/cm$^2$) activation of photosensitizers is used to generate reactive oxygen species that can damage the vasculature and kills cells [21], [22]. Photodynamic therapy has historically been approved for the treatment of superficial diseases beneath the skin or in the lining of organs where a light source can reach [23]. With the advancement of fiber optic light conduits, there is now the clinical possibility for photodynamic therapy to treat and permeabilize tumors that have grown deeply into the skin or other organs via intraoperative, endoscopic or interstitial procedures [24]. In fact, surgery immediately followed by photodynamic therapy has already been studied in the clinic for brain tumors (NCT03048240, NCT03897491, NCT00003788) [25], [26]. A single adjunctive dose of photodynamic therapy has been shown to add up to 18 months to the lifespan of patients with glioblastoma [27]. Despite the promising preclinical and clinical results using photodynamic therapy to permeabilize the BBB and treat brain tumors, the side effects of photodynamic therapy, including edema and neurotoxicity, remain a major concern in the clinic [28]-[31]. To address this issue, we have introduced photodynamic priming (PDP) which operates at low doses of optical energy and photosensitizer (i.e., < 1 μM × J/cm$^2$) to modulate biomolecular targets without killing the organism [32]. We have shown that PDP improves vascular permeability and enhances ONIVYDE® (liposome irinotecan, nal-IRI) extravasation into pancreatic tumor parenchyma by up to 11-fold without damaging surrounding healthy pancreas [32]. A combination of PDP and ONIVYDE® inhibited tumor growth, reduced metastasis, and doubled the median progression-free survival in pancreatic cancer mouse models [32]-[35]. While encouraging results have been obtained with PDP for pancreatic cancer treatment, there is work to be done to ensure that PDP can be used to disassociate the endothelium of the BBB that has a particularly high degree of junctional tightness.

It is increasingly clear that the presentation of junctional protein (i.e., pattern, geometrical organization, edge-presentation) and cell morphology plays an important role in regulating the permeability of cerebral endothelium [36]-[40]. Despite that information, the impact of sub-cytotoxic photochemistry on the presentation of junctional protein remains relatively understudied, presumably due, in part, to the lack of reliable quantitative analysis routines. Here, for the first time, we utilized a novel Junction Analyzer Program [37], [41] to quantify junction phenotype in response to PDP at various light energy densities using human brain microvascular endothelial cells (HBMECs). Images of immuno-stained ZO-1 and VE-cadherin were analyzed using the Junction Analyzer Program to calculate the percent of the cell perimeter presenting continuous, punctate, or perpendicular junctions before and after PDP. Furthermore, a transwell permeability assay was used to demonstrate that BBB

permeability to fluorescein isothiocyanate–dextran (FITC-dextran) or rhodamine-loaded nanoliposomes (rhodamine-nanoliposome) can be precisely controlled via light activation.

## II. Materials and Methods

### A. Cell Culture

Primary HBMECs were purchased from Cell Systems (ACBRI 376) and cultured as previously described [40]. Briefly, cells were cultured in flasks coated with 0.1% gelatin and grown in RPMI-1640 medium supplemented with 20% fetal bovine serum, 1% penicillin-streptomvcin, 2 mM L-glutamine (Thermo Fisher Scientific, Waltham, MA), 30 μg/mL endothelial cell growth supplement (ECGS) (Millipore Sigma, Burlington, MA), and 100 μg/mL heparin (Millipore Sigma) at 37 °C, with 5% $CO_2$. Cells were used for experiments within 7–10 passages. Cells arrived mycoplasma-free and were tested and found to be mycoplasma-free approximately 6 months later using the MycoAlert PLUS Mycoplasma Detection Kit (Lonza, LT07–701).

### B. Substrate Coating and Experimental Conditions

On day 1 of experiments, glass bottom 24-well plates (662892, Greiner Bio-One, Kremsmünster, Austria) or transwell inserts (24 well format, 1.0 μm pore size, Falcon, Abilene, TX) were respectively coated with 175 μL or 35 μL of 100 μg/mL fibronectin (F2006, Sigma Aldrich, St. Louis, MO) for 30 minutes at 37 °C. After coating, the excess fibronectin was removed, and the surfaces were rinsed with 37 °C phosphate-buffered saline (PBS). Cells were seeded at a density of $5\times10^4$ cells/$cm^2$ and then cultured for 5–9 days. On days 2–10, cells were treated with medium containing cAMP supplements: 250 μM of 8-CPT-cAMP (Abcam, ab120424) and 17.5 μM of RO-20-1724 (0415, Tocris Bioscience, Bristol, United Kingdom). Once supplemented medium was introduced to the cells, all of the following medium changes contained the supplements.

### C. Cell Viability and Metabolic Activity Assays, and Immunostaining

Briefly, on day 1 of experiments, HBMECs were plated at $5\times10^4$ cells/$cm^2$ within fibronectin-coated glass-bottom plates. The following day, the cAMP supplemented medium was introduced to the system and cells were grown for 48 hours to confluency. On day 4, cells were incubated with 0.25 μM of photosensitizer benzoporphyrin derivative (BPD, U.S. Pharmacopeia, Rockville, MD) in the supplemented medium for 24 hours. On day 5, prior to PDP, cells were washed twice with PBS and the fresh supplemented medium was added to each well. For PDP, cells were irradiated with 690 nm red light (0–5 J/$cm^2$, 6 mW/$cm^2$, bottom illumination). Light activation was performed using the ML6600 series laser system (690±5 nm; 1.5 W max output power; SMA fiber output with SMA905 connector, Modulight, Tampere, Finland). Cell metabolic activity and cell viability were determined via 3-(4,5-dimethylthiazol-2-yl)-2,5-diphenyltetrazolium bromide (MTT) assay and LIVE/DEAD® staining, respectively, at 24 hours or 72 hours after PDP. Surviving cells for PDP treated samples were normalized to a no treatment control. Cell confluency is defined as the number of cells stained with Calcein AM per frame, normalized to the no treatment control. Cell morphology was assessed 90 minutes after PDP (see Junction analysis).

### D. Immunostaining of Junction Proteins

At 90 minutes after PDP, HBMECs were rinsed with 37 °C PBS and fixed with 1% formaldehyde in PBS (Thermo Fisher Scientific) for 20 minutes. Prior to permeabilizing the cell membrane for 5 minutes with 0.25% TritonX-100 (Sigma-Aldrich) in PBS, cells were washed three times for 5 minutes each, with room temperature PBS. After permeabilization, the PBS wash steps were repeated and the samples were blocked for 1 hour at room temperature with 2% goat serum (Abcam, Cambridge, United Kingdom) in PBS. Cells were incubated with primary antibodies against ZO-1 (rabbit polyclonal IgG, Thermo Fisher Scientific, 61–7300, 1:500) and VE-cadherin (mouse monoclonal IgG, Santa Cruz, sc-9989, 1:50) in 2% goat serum overnight at 4°C. The following day, cells were washed and blocked in 2% goat serum for 1 hour. Cells were incubated with secondary antibodies goat anti-rabbit Alexa Fluor 488 (Abcam, ab150077, 1:100) or goat anti-mouse Alexa Fluor 568 (Thermo Fisher Scientific, A-11004, 1:100), and Hoechst (Thermo Fisher Scientific, H3570, 1:2500 or 4 μg/mL), in PBS for 1 hour at room temperature. Cells were washed prior to imaging. Note that all steps were performed under gentle rocking.

### E. Microscopy

For the LIVE/DEAD® assay, samples were imaged using the Lionheart (BioTek) at 20X. For cell-cell junction experiments (fixed-cell), samples were imaged using a 60X oil objective on an inverted microscope (IX83 Olympus microscope, Olympus cellSens Software). Images were captured using the red, green, and blue filters. Images shown within the manuscript were enhanced via ImageJ for better visualization of the cell-cell junction.

### F. Junction Analysis

Cell morphology and cell-cell junction organization were quantified using the Junction Analyzer Program, available for download at https://github.com/StrokaLab/JAnaP. Briefly, the cell perimeter was traced via “waypointing” for ZO-1 images (green fluorescent channel, A488) which were then projected onto the images of VE-cadherin (red fluorescent channel, A568), as previously described in [41]. To isolate ZO-1 and VE-cadherin, threshold values of 15 and 5 were applied, respectively. Further guidance on how to identify threshold values can be found in the supplement of [37] and in the Junction Analyzer Program User-Guide available using the link above. Next, the cell morphological parameters, including area, solidity, and circularity, were calculated. Specifically, solidity equals the area of the cell divided by the area of the convex (Supplementary Fig. 1a). Circularity equals $4\pi$ times the cell area divided by the cell perimeter squared (Supplementary Fig. 1b). Junction morphology was quantified by calculating the percent of the cell edge presenting continuous or perpendicular junction [41]. The specific phenotypes were classified based on the length of the junction that overlapped the cell edge (> 15 pixels for continuous junction) and the relative aspect ratio with respect to the cell edge (> 1.2 pixels for perpendicular junction, otherwise punctate). These values served as constant parameters when using the Junction Analyzer Program.

### G. Western Blot Analysis

VE-cadherin expression was analyzed using a standard Western blot analysis protocol (Bio-Rad). Briefly, HBMECs were seeded at a density of $5\times10^4$ cells/cm$^2$ within fibronectin-coated 35 mm petri dishes and grown to confluency. On day 2, cAMP supplemented medium was added to the cells. On day 4, cells were incubated with 0.25 μM BPD in the supplemented medium for 24 hours. On day 5, prior to PDP, cells were washed twice with PBS and the fresh supplemented medium was added to wells. For PDP, cells were irradiated with 690 nm red light (0 J/cm$^2$ or 1.2 J/cm$^2$, 6 mW/cm$^2$). Prior to collection, cells were washed thrice with cold PBS. Lysates were collected 90- and 24-hours post PDP by scrapping the cells off the petri dish within cold PBS. After centrifugation, cells were lysed with cold radioimmunoprecipitation assay (RIPA) buffer containing IX protease and phosphatase inhibitor cocktail (Thermo Fisher Scientific). The total protein from cell lysates was quantified using a Bichoninic acid (BCA) protein assay (Thermo Fisher Scientific). Cell lysates (20 μg) were separated on precast 4–12% Bis-Tris protein gels (NuPAGE) and electrotransferred onto PVDF membrane (Thermo Fisher Scientific). Membranes were blocked either with 5% milk/TBST or 5% BSA/TBST solution, for VE-cadherin and GAPDH, respectively. Proteins were sequentially detected using an anti-VE-cadherin antibody (1:1000, Santa Cruz sc-9989) according to the manufacturer's guidelines. GAPDH (1:500, Cell Signaling #2118) was used as the loading control. Visualization of protein bands was achieved using chemiluminescence (SuperSignal, Thermo Fisher Scientific). The membranes were imaged with the FluorChem E System (ProteinSimple, San Jose, CA). Quantitative analysis of protein expression was done using ImageJ software.

### H. Liposome Synthesis and Characterization

Nanoliposomes, fluorescently labeled with rhodamine, were synthesized via freeze-thaw extrusion as described previously [32], [34]. Briefly, dipalmitoylphosphatidylcholine (DPPC), cholesterol, distearoylphosphatidylethanolamgureinemethoxy polyethylene glycol (DSPE-PEG) and 1,2-dioleoylsn-glycero-3-phospho-(1'-rac-glycerol) (DOPG) (Avanti Polar Lipids, Alabaster, AL, USA) were codissolved with 1,2-dipalmitoyl-sn-glycero-3-phosphoethanolamine-N-(lissamine rhodamine B sulfonyl) (16:0 Liss Rhod PE) in chloroform. A thin film was created via rotary evaporator overnight. The film was rehydrated with 1 mL of deionized water. The lipid suspension was subjected to freeze-thaw cycles (4–45°C). The dispersions were extruded through polycarbonate membranes (0.1 μm pore size) at 42°C to form unilaminar vesicles. The final concentration of the rhodamine was checked using a fluorescence standard curve measured using a BioTek Synergy Neo2 plate reader (Excitation/Emission: 560/596 nm). The Omni (Brookhaven, Holtsville, NY, USA) measured particle size of monodispersed rhodamine-nanoliposomes to be ~100 nm in diameter (Supplementary Table 1).

### I. Transwell Permeability Assay

For permeability studies, HBMECs ($5\times10^4$ cells/cm$^2$) were seeded on transwell inserts that had been pre-coated with fibronectin. On the next day, cAMP supplemented medium was added, and cells were allowed to grow to confluency. On day 2 or 4, BPD (0.25 μM)-containing medium was added to the upper chamber for 24 hours of incubation. Following

this, cells were washed twice with PBS, fresh medium was added, and light was delivered to initiate PDP (690 nm, 0.6 J/cm$^2$ or 1.2 J/cm$^2$, 6 mW/cm$^2$, bottom illumination). Immediately following PDP, 400 μL of FITC-Dextran (1 mg/mL, 70 kDa, Sigma-Aldrich) or rhodamine-loaded liposomes (5 μM) was added to the upper (apical) chamber and allowed to diffuse across the membrane into the lower (basolateral) chamber. At different time points, the medium in the lower chamber was collected and the fluorescence signal was measured using a BioTek Synergy Neo2 plate reader (Excitation/Emission: 492/518 nm for FITC, or 560/596 nm for rhodamine). When evaluating the permeability of FITC-Dextran, on each of the following time points, the upper chamber was replenished with 400 μL of fresh FITC-dextran solution (1 mg/mL) and the lower chamber was also replenished with fresh medium (800 μL), in order to continue daily permeability evaluation. When evaluating the permeability of rhodamine-loaded liposomes, 30 minutes prior to collection, the upper chamber was replenished with 400 μL of fresh rhodamine-loaded liposomes (5 μM) and the lower chamber was replenished with fresh medium (800 μL). The apparent permeability coefficients (Papp, cm/min) of FITC-dextran solution (1 mg/mL) or rhodamine-loaded liposomes (5 μM) were from the following equation:

$$P_{app} = V_r \times (dC/dt)/(C_0 \times A) \quad (1)$$

$V_r$ is the volume of the basolateral chamber (cm$^3$). dQ/dt is the slope of the cumulative concentration of the FITC-dextran (or rhodamine-nanoliposome) in the basolateral chamber over time (μmol/L/min). $C_0$ is the initial concentration of FITC-dextran (or rhodamine-nanoliposome) in the apical chamber (μmol/L). A is the membrane surface area of the inserts (cm$^2$).

## III. Results and Discussions

### A. Sub-Cytotoxicity of PDP in HBMECs

For safe and effective drug delivery to the brain, it is of paramount importance to disrupt the BBB locally and transiently without causing endothelial cell death or vascular shutdown. Typically, photodynamic therapy involves the high optical energy (e.g., 80–300 J/cm$^2$) activation of photosensitizers in order to produce sufficient $^1O_2$ that can collapse the vasculature and induce cell apoptosis or necrosis [23], [43]-[48]. Recently, we have shown that PDP, with slightly lower optical energy (75 J/cm$^2$) and BPD photosensitizer, can improve vasculature permeability to nanomedicine in pancreatic tumors without causing normal tissue damage [32]-[35]. Other groups have shown the ability to permeabilize the BBB within mice using lower optical energies (10–40 J/cm$^2$) and the prodrug 5-aminolevulinic acid, however, vascular damage and edema often occur [28], [49], [50]. In this study, we used LIVE/DEAD® assay and MTT (metabolic-based) assay to determine the threshold of PDP in HBMECs *in vitro*. To recapitulate the in vivo basement membrane and enhance the brain endothelial phenotype, HBMECs were plated on fibronectin and treated with 8-(4-chlorophenylthio) adenosine-3',5'-cyclic monophosphate sodium salt (CPT-cAMP) and 4-(3-butoxy-4-methoxybenzyl) imidazolidin-2-one (RO-20-1724). The basal lamina fibronectin protein was selected over 7 other extracellular matrix components based on our prior work that showed fibronectin-coating results in the greatest HBMEC cell-cell

junction expression [40], [51]. cAMP and RO-20-1724 were introduced to enhance the junction phenotype, inhibit Rho/ROCK signaling in endothelial cells, and limit the formation of stress fibers by blocking myosin light chain phosphorylation [37], [40], [52].

Here, freeform BPD was incubated with HBMECs at a concentration of 0.25 μM for 24 hours prior to 690 nm light activation (0–5 J/cm$^2$, 6 mW/cm$^2$). At 24 hours post-PDP, the viability of HBMECs was assessed by LIVE/DEAD® assay. In a separate study, 72 hours post-PDP, mitochondrial activity was determined via MTT assay. Fig. 1 shows that PDP at light doses of ≤ 2.5 J/cm$^2$ had minimal effects on the viability and metabolic activity of HBMECs. At 5 J/cm$^2$, PDP significantly decreased the mitochondrial activity by 35.7±6.4% (Fig. 1a), induced 17.7±6% cell death (Fig. 1b), and reduced the confluency of HBMECs by 63.6% (Fig. 1c, Supplementary Fig. 2). It is well established that BPD localizes to the mitochondria and induces depolarization of mitochondrial membrane potential efficiently upon light illumination in cells [53]-[55]. Therefore, it is not surprising that PDP-treated HBMECs experience a larger loss in mitochondrial activity (by MTT assay) than cell membrane integrity (by LIVE/DEAD®). Based on these results, optical energies of 0.06, 0.3, 0.6, and 1.2 J/cm$^2$ (at a fixed irradiance of 6 mW/cm$^2$) were selected for the following experiments, while the concentration of BPD is fixed at 0.25 μM.

## B. PDP Slightly Alters Cell Morphology and F-actin Organization

To better understand how PDP impacts the brain endothelium, we first examined the impact of PDP on HBMEC morphology (i.e., area, solidity, and circularity) and F-actin organization using the well-established Junction Analyzer Program. We observed that PDP (0.06–1.2 J/cm$^2$) moderately increases the circularity and solidity of HBMECs by 3–13%, suggesting cells were under stress (Fig. 2a,b). However, this increase is modest compared to dying cells (cells treated with 5 J/cm$^2$) that had on average a 23.5% increase in circularity (data not shown). PDP did not impact the HBMECs area (Fig. 2c) nor perimeter (Supplementary Fig. 3). At the higher light doses of 0.6 and 1.2 J/cm$^2$, PDP induced F-actin reorganization from cortical bands near the cell edge to stress fibers throughout the HBMECs (Fig. 2d). It appeared VE-cadherin also showed a change in morphology, which motivated us to investigate further. Our new findings agree with previous observations by Ota et al. and others, which showed that the reactive oxygen species produced by photodynamic therapy can induce morphological changes and actin stress fiber formation in human umbilical vein endothelial cells [36], [56], [57]. Further, these reports showed that actin stress fiber reorganization from cortical bands to stress fibers in human umbilical vein endothelial cells was also accompanied by the mislocalization of VE-cadherin [36].

## C. PDP Alters the Endothelial Cell-Cell Junction Morphology

Among the 40 different transmembrane and scaffold proteins that form an endothelial cell-cell junction in the brain, VE-cadherin and ZO-1 are two of the important and foundational proteins that regulate BBB permeability. VE-cadherin is the primary transmembrane structural adhesive protein present in adherens junctions of HBMECs, prior to the formation of tight junctions, thus deeming it the junctional backbone [58]-[60]. ZO-1 is a scaffolding protein that regulates the recruitment and assembly of tight junction proteins (e.g., occludens and claudins) at the cytoplasmic surface of intercellular junctions [61]. It is also well

established that rearrangement of VE-cadherin and ZO-1 regulates vascular permeability [62]-[66]. As cell-cell junctions mature, VE-cadherin and ZO-1 reorganize from a serrated perpendicular geometry to a continuous strand linear to the cell edge [39], [40], [67].

We next investigated whether PDP could reverse the maturity of endothelial cell-cell junction through the rearrangement of VE-cadherin and ZO-1. Similar to the previous experiments, HBMECs were seeded in fibronectin-coated wells and treated with cAMP to start with mature cell-cell junctions [40]. Specifically, we examined the percentage of junction coverage per cell, as well as the pattern of junctions present at the cell edge (i.e., continuous mature junctions, perpendicular immature junctions, or punctate immature junctions) (Fig. 3a). Representative fluorescence images (Fig. 3b) show that PDP can reduce junctional coverage at the edge of the cell and significantly alter junction morphology. The changes in the HBMEC junction phenotype in response to PDP at various light energy densities (fluences) were further quantified using Junction Analyzer Program as described by us previously (Fig. 4). Junction Analyzer Program analysis revealed that PDP modestly reduced the coverage of VE-cadherin (72.4±0.8%) and ZO-1 (64.6±0.7%) at the cell edge by 10–20% in a light dose-dependent manner (Fig. 4a, b). This decrease in junctional coverage induced by PDP was accompanied by changes in junction morphology. We found that PDP not only decreases the mature VE-cadherin continuous junctions by ~17% (from 56.58±1.13% to 46.71±1.33%) (Fig. 4c) but also increases the immature VE-cadherin perpendicular junctions by ~46% (from 7.91±0.26% to 11.61±0.38%) in a light dose-dependent manner (Fig. 4e). Similar trends were observed with ZO-1, where PDP decreases the mature ZO-1 continuous junctions by ~27% (Fig. 4d) and increases the immature ZO-1 perpendicular junctions by ~38% at 1.2 J/cm$^2$ (Fig. 4f). Further analysis revealed that PDP (0.3–1.2 J/cm$^2$) increases the protrusion length (e.g., tip-to-tip distance [41]) of ZO-1 perpendicular junction, but not VE-cadherin perpendicular junction (Supplementary Fig. 4). The changes in perpendicular junction protrusion could be a result of F-actin stress fibers pulling on the connected tight junction proteins (ZO-1), but not adherens junction proteins (VE-cadherin). It has been reported by others that photodynamic therapy could cause the internalization of VE-cadherin and intercellular gaps, resulting in the disappearance and discontinuous junctions at the cell edge [36]. Interestingly, PDP did not significantly alter the amount of punctate, or dotted, junctions for VE-cadherin and ZO-1 ($p > 0.05$) (Fig. 4g, h). The number of punctate junctions was most likely unchanged after PDP, as cells were able to remain in constant contact with each other.

Previous reports have shown that endothelial monolayer confluency impacts VE-cadherin expression and pattern [68]-[70]. Zhang et al. also showed that photodynamic therapy downregulates the expression of VE-cadherin at the BBB in mice [50]. If PDP induced large gaps in the cell monolayer, as a result of cell death, it is speculated that the downregulation of VE-cadherin would occur via clathrin-coated endosomal internalization [71]. Here, western blot analysis shows that PDP did not significantly alter the expression of VE-cadherin in HBMECs (Supplementary Fig. 5). The above results demonstrate that PDP not only induces cellular stresses as evident by increased stress fiber formation, roundness, and solidity, but also promotes morphological changes to junction proteins. Most importantly, PDP can shift a stable endothelial monolayer into an immature state while maintaining HBMEC viability.

### D. PDP Induces HBMEC Permeability to FITC-dextran

We have previously demonstrated that the number of discontinuous VE-cadherin and ZO-1 junctions correlates positively with HBMEC permeability [40]. Similarly, Li et al. showed that a change in the pattern of ZO-1 (from “linear” junction to a “discontinuous, segmented and dotted” phenotype) is associated with increased permeability in HBMECs [52]. Knowing that PDP can modulate the morphology of cell-cell junctions (Fig. 3 and 4), we next examined the ability of PDP to improve HBMEC permeability to FITC-dextran or rhodamine-nanoliposomes using a transwell model. At different time points after PDP, the amount of FITC-dextran (or rhodamine-nanoliposome) that diffuses from the apical chamber into the basolateral chamber was quantified using a plate reader and the apparent permeability coefficient ($P_{app}$, cm/min) was calculated.

Without PDP (0 J/cm$^2$), a baseline diffusion of FITC-dextran into the basolateral chamber was observed (Fig. 5a). The average $P_{app}$ of FITC-dextran is ~$7.5\times10^{-5}$ cm/min, similar to that observed by others (Fig. 5b) [72], [73]. By day 7, the $P_{app}$ of FITC-dextran in the untreated HBMECs control group began to increase. This observation is consistent with other’s reports showing that prolonged activation of cAMP may cause a delay in the repression of Ras-related protein (R-Ras), resulting in the disruption of VE-cadherin and endothelial cell barriers [74]. PDP at 0.6 J/cm$^2$ and 1.2 J/cm$^2$ significantly improved the diffusion of FITC-dextran across the HBMEC monolayer by ~2.6-fold and 4-fold, respectively, in a dose-dependent manner (Fig. 5a). The $P_{app}$ of FITC-dextran was found to be the highest at 2–3 days post-PDP. On day 2, transwells primed with 1.2 J/cm$^2$ had approximately 40.86% of their starting FITC-dextran diffuse into the basolateral chamber. By days 6 and 9, the $P_{app}$ of FITC-dextran in the PDP groups (0.6 and 1.2 J/cm$^2$) were found to be similar to that of the control group (0 J/cm$^2$). The transwell models that received the higher optical energy (1.2 J/cm$^2$) took an additional 3 days to recover presumably due to increased cell contractility and number of immature junctions. Although this was an *in vitro* model, our findings are consistent with previous *in vivo* findings showing that PDP-assisted endothelial opening persists at least up to 3 days [32]. These results also suggest that PDP dose can be customized to control the degree and duration of endothelium permeabilization.

We have previously shown that PDP can improve the permeability of ‘leaky’ tumor vasculature to nanoliposomes by 11-fold *in vivo* [32]. We next tested if PDP also improved rhodamine-nanoliposomes, ~100 nm in diameter (Supplementary Table 1), penetration across the HBMEC monolayer cultures that have a particularly high degree of junctional tightness. The permeability of rhodamine-nanoliposomes was monitored up to ~48 hours (Fig. 6), as the clinically relevant nanoliposomes typically have a circulation half-life of 24–48 hours [75], [76]. Without PDP (0 J/cm$^2$), the average $P_{app}$ of rhodamine-nanoliposomes is ~$1.1\times10^{-7}$ cm/min. PDP at 0.6 J/cm$^2$ significantly improved the $P_{app}$ of rhodamine-nanoliposomes by 14.6-, 9.8-, and 5.0-fold at 1, 25, and 49 hours, respectively, compared to the control (0 J/cm$^2$). This improvement in the $P_{app}$ of rhodamine-nanoliposomes was even more pronounced when using PDP and 1.2 J/cm$^2$ (38.5-, 18.1-, and 11.5-fold at 1, 25 and 49 hours, respectively). We observed that only less than 0.09% of the rhodamine-liposomes diffused into the basolateral chamber. This tightness properties displayed in our model was found similar to others *in vitro* model [77]. At 1.2 J/cm$^2$, PDP facilitated the leakage of up to

3.43% of the liposomes into the basolateral chamber over a 30-minute incubation period. This significant (30-fold) improvement in drug penetration across the endothelial barrier suggests that PDP is a promising modality for enhancing drug devilry across the BBB *in vivo*, where less than 0.14%ID/g of the injected liposomes can cross the rat BBB [78]-[82]. While 5-aminolevulinic acid-mediated photodynamic therapy and focused ultrasound [36], [83], [84] can also improve the drug delivery across the endothelial monolayer by 2- to 5.3-fold, these modalities are often cytotoxic and can potentially lead to undesired normal tissue destruction.

This is the first study to demonstrate that PDP can significantly improve endothelial permeability to both macromolecules and nanoparticles in a transwell model. The uniqueness of PDP lies in its spatiotemporal selectivity, which offers the opportunity to confine endothelial permeabilization to the site where the light is directed. This spatiotemporal control of PDP may further reduce normal brain tissue damages and warrants further investigation in animals. In the clinic, we believe the most advantageous and safe initial application of PDP is following brain tumor resection while patients are in the operating room. In this context, patients will receive PDP intraoperatively via fiber optic light conduits placed within the resection cavity [25], [26]. The forward-looking goal of photodvnamic therapy is to reversibly open the BBB for enhanced drug delivery and to sterilize unresectable tumor cells during open surgery, while sparing normal brain tissue and the healthy vasculature. These unresectable infiltrating glioblastoma cells have been shown to cause an 80% recurrence within 1–2 cm of the original tumor edge [85], [86]. While it is true that light penetration depth (i.e., the depth at which the incident optical energy drops to 37%, 1/e) is typically 1–4 mm in the brain, we have recently shown that diffused red light (i.e., the remaining 37% optical energy) can reach up to 1.5–2 cm deep in rat brains to activate BPD for PDP [87]. This suggests that intraoperative PDP is sufficient to manage brain diseases that are 1–2 cm in depth (e.g., the unresectable, invasive margin of most brain cancers). For deeper brain tissues, light can be delivered to the entire target using stereotactically placed fibers in the clinic (similar to laser probes currently used for interstitial thermotherapy) [88]-[92]. In this study, the clinically relevant, longer wavelength photosensitizer, BPD, (690 nm, deeper light penetration) was selected for PDP. This is an alternative to 5-aminolevulinic acid (Gliolan®)-induced protoporphyrin IX (635 nm), which is currently approved for fluorescence-guided surgery of brain tumors [93], [94] and is generally reserved for treating topical lesions [23], [95]. In fact, we have shown that 690 nm light activation of BPD induces PDP effects at further depths in rat brain (1.5–2 cm), compared to 635 nm light activation of protoporphyrin IX (≤ 1 cm) [87]. Therefore, an immediate future direction would be to compare the efficacy of PDP for BBB opening using both FDA-approved BPD and Gliolan® *in vivo*.

## IV. Conclusion

In summary, the complexities of the brain necessitate the innovation of a drug delivery strategy capable of overcoming the neurovascular unit while leaving normal brain cells undamaged. An emerging paradigm in brain drug delivery suggests that stimuli-responsive strategies can more accurately control BBB permeability at the right time, right place, and for the appropriate duration. Both photodynamic therapy and focused ultrasound hold great

clinical promise for overcoming the BBB. However, their cytotoxic nature and associated adverse events limit the clinical application and efficacy of drug delivery. To address these challenges, we applied a sub-lethal, photodynamic priming modality to reverse the mature brain endothelial cell–cell junction. The photodynamic priming approach is inspired by recent advances in tumor vascular permeabilization, which improves drug delivery to pancreatic tumors. Here, for the first time, we showed that PDP could significantly alter the endothelial cell–cell junction phenotype (i.e., continuous, punctate, or perpendicular), and improve nanoparticle penetration across the tight endothelium by up to 30-fold. Future work will involve further characterization of multi-cycle PDP in cells and in animal models and will address the benefit of using a longer wavelength photosensitizer. The impact of PDP on other components of the neurovascular unit (e.g., pericytes, neurons), as well as the photosensitizer-light interval, will also be the subject of future studies. Building on our successes using PDP for pancreatic cancer treatment, this study opens up new avenues for developing brain targeting drug delivery systems.

## Supplementary Material

Refer to Web version on PubMed Central for supplementary material.

## Acknowledgment

The authors would like to acknowledge Kyle Thomas at Yellow Basket, LLC (kyle@yellowbas-ket.io) for Junction Analyzer Program software development support, and the University of Maryland.

This work is supported by the Burroughs Wellcome Career Award at the Scientific Interface (KMS), the Fischell Fellowship in Biomedical Engineering (KMG), the ASPIRE Scholarship from the Maryland Technology Enterprise Institute (JWJ, JS), the National Institutes of Health (NIH) R00CA194269 grant (HCH), the NIH R21EB028508 grant (HCH), the UMD-UMB Research and Innovation Seed Grant (HCH), the University of Maryland Strategic Partnership (MPower) Fellowship (SV), and the University of Maryland.

## Biographies

**Collin T. Inglut** received a B.S. degree in biomedical engineering from the Rochester Institute of Technology, Rochester, NY, in 2017. He is expected to complete a Ph.D. in bioengineering from the University of Maryland, College Park, in May of 2022.

From 2013–2016 he completed 3 co-ops at the medical device company, Zimmer Biomet, and was a summer research intern at George Maison University. Since 2017, he has been a member of the Optical Therapeutics & Nanotechnology Laboratory at the University of Maryland, College Park. He is an author of 5 articles and a book chapter. His current research focuses on developing nanotechnology platforms that leverage photodynamic therapy to modulate the blood-brain barrier and treat glioblastoma.

Mr. Inglut is a member of the International Photomedicine Association and the Biomedical Engineering Society. He is a recipient of the UMD-NCI Partnership for Integrative Cancer Research fellowship.

**Kelsey M. Gray** received a B.Ch.E degree from the University of Delaware, Newark, DE in 2012, and a Ph.D. degree in Bioengineering from the University of Maryland, College Park, MD, in 2019.

From 2009 to 2012, she was a Summer Research Intern in the Payne Laboratory in the Institute for Bioscience and Biotechnology Research at the University of Maryland. She then worked as a Remediation Engineer in the Technical Professional Development Program at Hospira in Rocky Mount, NC until 2014, before serving as a Graduate Research Assistant in the Cell and Microenvironment Engineering Laboratory until 2019. She is currently a Senior Scientist at Pfizer, Pearl River, NY. She has authored almost 15 publications and delivered over 20 presentations at national and international conferences and local symposiums. Her research interests include vascular mechanobiology, cell-cell junctions, and the blood-brain barrier; as well as biomaterials and electrodeposition.

Dr. Gray's awards and honors include the Fischell Fellowship in Biomedical Engineering (Fischell Department of Bioengineering, University of Maryland, 2014–2019), the Dr. Mabel S. Spencer Award for Excellence in Graduate Achievement (The Graduate School, University of Maryland, 2017), and the Cellular and Molecular Bioengineering Graduate Student Shooting Star Award (Biomedical Engineering Society, 2017 and 2018).

**Shruti Vig** completed her baccalaureate in biomedical engineering from SASTRA University, Tamil Nadu, India, in 2017. Shruti is presently a Ph.D. student at the Fischell Department of Bioengineering, University of Maryland, College Park.

From 2017–2018, she worked as a research trainee in the renal division at the Harvard Institute of Medicine. She joined the Optical Therapeutics & Nanotechnology Laboratory at the University of Maryland, College Park, in 2019. Her current research focuses on employing nanotechnology platforms along with sonodynamic therapy to target the blood-brain tumor barrier.

Ms. Vig is a recipient of the MPower Doctoral Fellowship.

**Jae W. Jung** is a third-year undergraduate student pursuing a B.S. degree in bioengineering at the University of Maryland, College Park, USA. He has been a part of the Cell and Microenvironment Engineering under Dr. Kimberly M. Stroka since 2018. He has received the ASPIRE Undergraduate Fellowship from University of Maryland in 2019.

**Jillian Stabile** is in the process of completing a B.S. degree in bioengineering from the University of Maryland College Park and will graduate in May 2020. She will be pursuing a career in biotechnology in Baltimore, Maryland.

From 2018 to 2020, she was a student researcher in the Huang Lab at the University of Maryland College Park within the Fischell Department of Bioengineering. Her research interests and projects related to improving drug delivery methods and mechanisms related to cancer therapy. She recently contributed to a project published in Journal of Clinical Medicine and a book chapter on gold nanoparticles.

Ms. Stabile was an ASPIRE Fellowship recipient where she further explored her research interests within the Huang Lab.

**Yuji Zhang** received both B.S. and M.S. degree in Biomedical Engineering from Southeast University, Nanjing, China, in 2000 and 2003 respectively. She received her Ph.D. degree in computer engineering from the Virginia Polytechnic Institute and State University in 2010.

From 2011 to 2014, she was an assistant professor of biomedical informatics at Mayo Clinic College of Medicine. In 2014, she joined the University of Maryland School of Medicine as the lead bioinformatician at the University of Maryland Greenebaum Comprehensive Cancer Center.

Dr. Zhang is currently an associate professor in the Department of Epidemiology and Public Health with over 60 peer-reviewed articles. Her research focuses on developing translational biostatistics and informatics approaches to reveal novel human disease mechanisms.

**Kimberly M. Stroka** received a B.S. degree in physics from Denison University, Granville, OH, in 2006 and a Ph.D. in bioengineering from the University of Maryland, College Park, MD, in 2011.

From 2011 to 2013, she was a postdoctoral fellow in the Institute for NanoBioTechnology at The Johns Hopkins University, Baltimore, MD. Since 2014, she has been an Assistant Professor in the Fischell Department of Bioengineering at the University of Maryland, College Park. She is the author of 33 articles and 3 book chapters. Her research interests include cell mechanobiology, cell mechanics, cell-cell interactions, cell-substrate interactions, cell migration, tumor cell metastasis, blood-brain barrier modeling, and microfabricated devices for modeling of cellular systems.

Dr. Stroka is a member of the Biomedical Engineering Society. She is a recipient of the NSF Graduate Research Fellowship, NIH F31 and F32 Fellowships, Burroughs Wellcome Career Award at the Scientific Interface, Biomedical Engineering Society Rita Schaffer Young Investigator Award, Outstanding Young Scientist Award from the Maryland Academy of

Sciences, Cellular and Molecular Bioengineering Young Innovator recognition, and NSF CAREER Award.

**Huang Chiao Huang** received a B.S. degree in Chemical Engineering from National Taipei University of Technology, Taiwan, in 2005 and a Ph.D. in Chemical Engineering from the Arizona State University, Tempe, AZ, in 2012.

From 2012 to 2018, he was a postdoctoral fellow in the Wellman Center for Photomedicine at Massachusetts General Hospital and Harvard Medical School, Boston, MA. Since 2018, he has been an Assistant Professor in the Fischell Department of Bioengineering at the University of Maryland, College Park. He is the author of 37 articles and 1 patent. His research interests include precision cancer nanomedicine, mechanism-based combination therapy, photodynamic therapy, and site-directed photochemistry and fluorescence diagnostics.

Dr. Huang is the councilor of the American Society for Photobiology and the member of the International Photodynamic Association. He is a recipient of the Tosteson & Fund for Medical Discovery Fellowship, NIH K99/R00 Pathway to Independence Award, and NIH NIBIB Trailblazer Award.

## References

[1]. Banks WA, “From blood-brain barrier to blood-brain interface: new opportunities for CNS drug delivery,” Nature Reviews Drug Discovery, vol. 15, no. 4, pp. 275–292, 2016/04/01, 2016. [PubMed: 26794270]

[2]. Chen Y, and Liu L, “Modern methods for delivery of drugs across the blood-brain barrier,” Advanced Drug Delivery Reviews, vol. 64, no. 7, pp. 640–665, 2012/05/15/, 2012. [PubMed: 22154620]

[3]. Daneman R, and Prat A, “The blood-brain barrier,” Cold Spring Harbor perspectives in biology, vol. 7, no. 1, pp. a020412–a020412, 2015. [PubMed: 25561720]

[4]. Pardridge WM, “The blood-brain barrier: bottleneck in brain drug development,” NeuroRx : the journal of the American Society for Experimental NeuroTherapeutics, vol. 2, no. 1, pp. 3–14, 2005. [PubMed: 15717053]

[5]. Obermeier B, Daneman R, and Ransohoff RM, “Development, maintenance and disruption of the blood-brain barrier,” Nature medicine, vol. 19, no. 12, pp. 1584–1596,2013.

[6]. Wevers NR, and de Vries HE, “Morphogens and blood-brain barrier function in health and disease,” Tissue barriers, vol. 4, no. 1, pp. e1090524–e1090524, 2015. [PubMed: 27141417]

[7]. Dong X, “Current Strategies for Brain Drug Delivery,” Theranostics, vol. 8, no. 6, pp. 1481–1493,2018. [PubMed: 29556336]

[8]. Luissint AC, Artus C, Glacial F, Ganeshamoorthy K, and Couraud PO, “Tight junctions at the blood brain barrier: physiological architecture and disease-associated dysregulation,” Fluids Barriers CNS, vol. 9, no. 1, pp. 23, 11 9, 2012. [PubMed: 23140302]

[9]. Hersh DS, Wadajkar AS, Roberts N, Perez JG, Connolly NP, Frenkel V, Winkles JA, Woodworth GF, and Kim AJ, “Evolving Drug Delivery Strategies to Overcome the Blood Brain Barrier,” Curr Pharm Des, vol. 22, no. 9, pp. 1177–1193, 2016. [PubMed: 26685681]

[10]. Neuwelt EA, Barnett PA, Bigner DD, and Frenkel EP, “Effects of adrenal cortical steroids and osmotic blood-brain barrier opening on methotrexate delivery to gliomas in the rodent: the factor of the blood-brain barrier,” Proceedings of the National Academy of Sciences of the United States of America, vol. 79, no. 14, pp. 4420–4423, 1982. [PubMed: 6289301]

[11]. Tsai H-C, Tsai C-H, Chen W-S, Inserra C, Wei K-C, and Liu H-L, “Safety evaluation of frequent application of microbubble-enhanced focused ultrasound blood-brain-barrier opening,” Scientific reports, vol. 8, no. 1, pp. 17720–17720,2018. [PubMed: 30531863]

[12]. Chu P-C, Liu H-L, Lai H-Y, Lin C-Y, Tsai H-C, and Pei Y-C, “Neuromodulation accompanying focused ultrasound-induced blood-brain barrier opening,” Scientific reports, vol. 5, pp. 15477–15477, 2015. [PubMed: 26490653]

[13]. Rapoport SI, “Osmotic Opening of the Blood-Brain Barrier: Principles, Mechanism, and Therapeutic Applications,” Cellular and Molecular Neurobiology, vol. 20, no. 2, pp. 217–230, 4 01, 2000. [PubMed: 10696511]

[14]. Brown RC, Egleton RD, and Davis TP, “Mannitol opening of the blood-brain barrier: regional variation in the permeability of sucrose, but not 86Rb+ or albumin,” Brain Res, vol. 1014, no. 1–2, pp. 221–7, 7 16, 2004. [PubMed: 15213006]

[15]. Vykhodtseva NI, Hynynen K, and Damianou C, “Histologic effects of high intensity pulsed ultrasound exposure with subharmonic emission in rabbit brain in vivo,” Ultrasound Med Biol, vol. 21, no. 7, pp. 969–79, 1995. [PubMed: 7491751]

[16]. Sheikov N, McDannold N, Sharma S, and Hynynen K, “Effect of focused ultrasound applied with an ultrasound contrast agent on the tight junctional integrity of the brain microvascular endothelium,” Ultrasound in medicine & biology, vol. 34, no. 7, pp. 1093–1104, 2008. [PubMed: 18378064]

[17]. Salford LG, Brun A, Sturesson K, Eberhardt JL, and Persson BR, “Permeability of the blood-brain barrier induced by 915 MHz electromagnetic radiation, continuous wave and modulated at 8, 16, 50, and 200 Hz,” Microsc Res Tech, vol. 27, no. 6, pp. 535–42, 4 15, 1994. [PubMed: 8012056]

[18]. Stam R, “Electromagnetic fields and the blood-brain barrier,” Brain Research Reviews, vol. 65, no. 1, pp. 80–97, 2010/10/05/, 2010. [PubMed: 20550949]

[19]. Appelboom G, Detappe A, LoPresti M, Kunjachan S, Mitrasinovic S, Goldman S, Chang SD, and Tillement O, “Stereotactic modulation of blood-brain barrier permeability to enhance drug delivery,” Neuro-Oncology, vol. 18, no. 12, pp. 1601–1609,2016. [PubMed: 27407134]

[20]. Sandor N, Walter FR, Bocsik A, Santha P, Schilling-Toth B, Lener V, Varga Z, Kahan Z, Deli MA, Safrany G, and Hegyesi H, “Low dose cranial irradiation-induced cerebrovascular damage is reversible in mice,” PLoS One, vol. 9, no. 11, pp. e112397, 2014. [PubMed: 25393626]

[21]. Celli JP, Spring BQ, Rizvi I, Evans CL, Samkoe KS, Verma S, Pogue BW, and Hasan T, “Imaging and photodynamic therapy: mechanisms, monitoring, and optimization,” Chem Rev, vol. 110, no. 5, pp. 2795–838, 5 12,2010. [PubMed: 20353192]

[22]. Sorrin AJ, Ruhi MK, Ferlic NA, Karimnia V, Polacheck WJ, Celli JP, Huang HC, and Rizvi I, “Photodynamic Therapy and the Biophysics of the Tumor Microenvironment,” Photochemistry and Photobiology, vol. 2, no. 96, pp. 232–259, 1 2 2020.

[23]. Zhao B, and He Y-Y, “Recent advances in the prevention and treatment of skin cancer using photodynamic therapy,” Expert review of anticancer therapy, vol. 10, no. 11, pp. 1797–1809,2010. [PubMed: 21080805]

[24]. Huang Z, “A review of progress in clinical photodynamic therapy,” Technology in cancer research & treatment, vol. 4, no. 3, pp. 283–293, 2005. [PubMed: 15896084]

[25]. Bechet D, Mordon SR, Guillemin F, and Barberi-Heyob MA, “Photodynamic therapy of malignant brain tumours: a complementary approach to conventional therapies,” Cancer Treat Rev, vol. 40, no. 2, pp. 229–41, 3, 2014. [PubMed: 22858248]

[26]. Mahmoudi K, Garvey KL, Bouras A, Cramer G, Stepp H, Jesu Raj JG, Bozec D, Busch TM, and Hadjipanayis CG, “5-aminolevulinic acid photodynamic therapy for the treatment of high-grade gliomas,” J Neurooncol, vol. 141, no. 3, pp. 595–607, 2, 2019. [PubMed: 30659522]

[27]. Kostron H, Obwegeser A, and Jakober R, “Photodynamic therapy in neurosurgery: a review,” Journal of Photochemistry and Photobiology B: Biology, vol. 36, no. 2, pp. 157–168, 1996/11/01/, 1996.

[28]. Hirschberg H, Uzal FA, Chighvinadze D, Zhang MJ, Peng Q, and Madsen SJ, “Disruption of the blood-brain barrier following ALA-mediated photodynamic therapy,” Lasers Surg Med, vol. 40, no. 8, pp. 535–42, 10, 2008. [PubMed: 18798293]

[29]. Ito S, Rachinger W, Stepp H, Reulen HJ, and Stummer W, “Oedema formation in experimental photo-irradiation therapy of brain tumours using 5-ALA,” Acta Neurochir (Wien), vol. 147, no. 1, pp. 57–65; discussion 65, 1, 2005. [PubMed: 15565479]

[30]. Henry Hirschberg MD, Even A-P, Signe S, Marlon Mathews MD, and Steen JM, “Increased brain edema following 5-aminolevulinic acid mediated photodynamic in normal and tumor bearing rats.” Proc.SPIE, vol. 6424, 2007.

[31]. Stummer W, Gotz C, Hassan A, Heimann A, and Kempski O, “Kinetics of Photofrin II in perifocal brain edema,” Neurosurgery, vol. 33, no. 6, pp. 1075–81; discussion 1081–2, 12, 1993. [PubMed: 8133993]

[32]. Huang HC, Rizvi I, Liu J, Anbil S, Kalra A, Lee H, Baglo Y, Paz N, Hayden D, Pereira S, Pogue BW, Fitzgerald J, and Hasan T, “Photodynamic Priming Mitigates Chemotherapeutic Selection Pressures and Improves Drug Delivery,” Cancer Res, vol. 78, no. 2, pp. 558–571, 1 15,2018. [PubMed: 29187403]

[33]. Pigula M, Huang HC, Mallidi S, Anbil S, Liu J, Mai Z, and Hasan T, “Size-dependent Tumor Response to Photodynamic Therapy and Irinotecan Monotherapies Revealed by Longitudinal Ultrasound Monitoring in an Orthotopic Pancreatic Cancer Model,” Photochem Photobiol, vol.95, no. 1, pp. 378–386,9 19, 2018. [PubMed: 30229942]

[34]. Huang HC, Mallidi S, Liu J, Chiang CT, Mai Z, Goldschmidt R, Ebrahim-Zadeh N, Rizvi I, and Hasan T, “Photodynamic Therapy Synergizes with Irinotecan to Overcome Compensatory Mechanisms and Improve Treatment Outcomes in Pancreatic Cancer,” Cancer Res, vol. 76, no. 5, pp. 1066–77, 3 1,2016. [PubMed: 26719532]

[35]. Anbil S, Pigula M, Huang HC, Mallidi S, Broekgaarden M, Baglo Y, De Silva P, Simeone DM, Mino-Kenudson M, Maytin EV, Rizvi I, and Hasan T, “Vitamin D receptor activation and photodynamic priming enable durable low-dose chemotherapy,” Mol Cancer Ther, 3 27, 2020.

[36]. Ota H, Matsumura M, Miki N, and Minamitami H, “Photochemically induced increase in endothelial permeablity regulated by RhoA activation,” Photochemical & Photobiological Sciences, vol. 8, no. 10, pp. 1401–1407, 2009. [PubMed: 19789809]

[37]. Gray KM, Katz DB, Brown EG, and Stroka KM, “Quantitative Phenotyping of Cell-Cell Junctions to Evaluate ZO-1 Presentation in Brain Endothelial Cells,” Annals of Biomedical Engineering, vol. 47, no. 7, pp. 1675–1687, 7 01, 2019. [PubMed: 30993538]

[38]. Onken MD, Mooren OL, Mukherjee S, Shahan ST, Li J, and Cooper JA, “Endothelial monolayers and transendothelial migration depend on mechanical properties of the substrate,” Cytoskeleton (Hoboken, N.J.), vol. 71, no. 12, pp. 695–706, 2014/12//, 2014.

[39]. Huveneers S, Oldenburg J, Spanjaard E, van der Krogt G, Grigoriev I, Akhmanova A, Rehmann H, and de Rooij J, “Vinculin associates with endothelial VE-cadherin junctions to control force-dependent remodeling,” The Journal of cell biology, vol. 196, no. 5, pp. 641–652,2012. [PubMed: 22391038]

[40]. Gray KM, Jung JW, Inglut CT, Huang HC, and Stroka KM, “Quantitatively relating brain endothelial cell-cell junction phenotype to global and local barrier properties under varied culture conditions via the Junction Analyzer Program,” Fluids Barriers CNS, vol. 17, no. 1, pp. 16, 2 11,2020. [PubMed: 32046757]

[41]. Pranda MA, Gray KM, DeCastro AJL, Dawson GM, Jung JW, and Stroka KM, “Tumor Cell Mechanosensing During Incorporation into the Brain Microvascular Endothelium,” Cell Mol Bioeng, vol. 12, no. 5, pp. 455–480, 10, 2019. [PubMed: 31719927]

[42]. Gilbertson RJ, and Rich JN, “Making a tumour’s bed: glioblastoma stem cells and the vascular niche,” Nat Rev Cancer, vol. 7, no. 10, pp. 733–6, 10, 2007. [PubMed: 17882276]

[43]. Dhillon SS, Demmy TL, Yendamuri S, Loewen G, Nwogu C, Cooper M, and Henderson BW, “A Phase I Study of Light Dose for Photodynamic Therapy Using 2-[1-Hexyloxyethyl]-2 Devinyl

Pyropheophorbide-a for the Treatment of Non-Small Cell Carcinoma In Situ or Non-Small Cell Microinvasive Bronchogenic Carcinoma: A Dose Ranging Study," Journal of thoracic oncology : official publication of the International Association for the Study of Lung Cancer, vol. 11, no. 2, pp. 234–241,2016.

[44]. Cloughesy TF, Cavenee WK, and Mischel PS, "Glioblastoma: From Molecular Pathology to Targeted Treatment," Annual Review of Pathology: Mechanisms of Disease, vol. 9, no. 1, pp. 1–25, 2014.

[45]. Azzouzi AR, Barret E, Bennet J, Moore C, Taneja S, Muir G, Villers A, Coleman J, Allen C, Scherz A, and Emberton M, "TOOKAD(R) Soluble focal therapy: pooled analysis of three phase II studies assessing the minimally invasive ablation of localized prostate cancer," World J Urol, vol. 33, no. 7, pp. 945–53, 7, 2015. [PubMed: 25712310]

[46]. Mahmoudi K, Garvey KL, Bouras A, Cramer G, Stepp H, Jesu Raj JG, Bozec D, Busch TM, and Hadjipanayis CG, "5-aminolevulinic acid photodynamic therapy for the treatment of high-grade gliomas," Journal of neuro-oncology, vol. 141, no. 3, pp. 595–607, 2019. [PubMed: 30659522]

[47]. Agostinis P, Berg K, Cengel KA, Foster TH, Girotti AW, Gollnick SO, Hahn SM, Hamblin MR, Juzeniene A, Kessel D, Korbelik M, Moan J, Mroz P, Nowis D, Piette J, Wilson BC, and Golab J, "Photodynamic therapy of cancer: an update," CA: a cancer journal for clinicians, vol. 61, no. 4, pp. 250–281, Jul-Aug, 2011. [PubMed: 21617154]

[48]. Zhu TC, Kim MM, Liang X, Finlay JC, and Busch TM, "In-vivo singlet oxygen threshold doses for PDT," Photonics Lasers Med, vol. 4, no. 1, pp. 59–71, 2, 2015. [PubMed: 25927018]

[49]. Semyachkina-Glushkovskaya O, Kurths J, Borisova E, Sokolovski S, Mantareva V, Angelov I, Shirokov A, Navolokin N, Shushunova N, Khorovodov A, Ulanova M, Sagatova M, Agranivich I, Sindeeva O, Gekalyuk A, Bodrova A, and Rafailov E, "Photodynamic opening of blood-brain barrier," Biomedical Optics Express, vol. 8, no. 11, pp. 5040–5048,2017. [PubMed: 29188101]

[50]. Zhang C, Feng W, Vodovozova E, Tretiakova D, Boldyrevd I, Li Y, Kürths J, Yu T, Semyachkina-Glushkovskaya O, and Zhu D, "Photodynamic opening of the blood-brain barrier to high weight molecules and liposomes through an optical clearing skull window," Biomedical optics express, vol. 9, no. 10, pp. 4850–4862, 2018. [PubMed: 30319907]

[51]. Baeten KM, and Akassoglou K, "Extracellular matrix and matrix receptors in blood-brain barrier formation and stroke," Developmental neurobiology, vol. 71, no. 11, pp. 1018–1039, 2011. [PubMed: 21780303]

[52]. Li B, Zhao W-D, Tan Z-M, Fang W-G, Zhu L, and Chen Y-H, "Involvement of Rho/ROCK signalling in small cell lung cancer migration through human brain microvascular endothelial cells," FEBS Letters, vol. 580, no. 17, pp. 4252–4260, 2006. [PubMed: 16828752]

[53]. Inglut CT, Baglo Y, Liang BJ, Cheema Y, Stabile J, Woodworth GF, and Huang HC, "Systematic Evaluation of Light-Activatable Biohybrids for Anti-Glioma Photodynamic Therapy," J Clin Med, vol. 8, no. 9, article number: 1269. 8 21, 2019.

[54]. Kessel D, and Luo Y, "Mitochondrial photodamage and PDT-induced apoptosis," J Photochem Photobiol B, vol. 42, no. 2, pp. 89–95, 2, 1998. [PubMed: 9540214]

[55]. Kessel D, "Photodynamic therapy: Promotion of efficacy by a sequential protocol," Journal of porphyrins and phthalocyanines, vol. 20, no. 1–4, pp. 302–306, Jan-Apr, 2016. [PubMed: 27528795]

[56]. Wilson C, and González-Billault C, "Regulation of cytoskeletal dynamics by redox signaling and oxidative stress: implications for neuronal development and trafficking," Frontiers in Cellular Neuroscience, vol. 9, no. 381, 2015-9-30, 2015.

[57]. Moldovan L, Mythreye K, Goldschmidt-Clermont PJ, and Satterwhite LL, "Reactive oxygen species in vascular endothelial cell motility. Roles of NAD(P)H oxidase and Racl," Cardiovascular Research, vol. 71, no. 2, pp. 236–246, 2006. [PubMed: 16782079]

[58]. Campbell HK, Maiers JL, and DeMali KA, "Interplay between tight junctions & adherens junctions," Experimental cell research, vol. 358, no. 1, pp. 39–44, 2017. [PubMed: 28372972]

[59]. Abu Taha A, and Schnittler H-J, "Dynamics between actin and the VE-cadherin/catenin complex: novel aspects of the ARP2/3 complex in regulation of endothelial junctions," Cell adhesion & migration, vol. 8, no. 2, pp. 125–135, 2014. [PubMed: 24621569]

[60]. Gavard J, and Gutkind JS, “VE-cadherin and claudin-5: it takes two to tango,” Nature cell biology, vol. 10, no. 8, pp. 883–885, 2008. [PubMed: 18670447]

[61]. Rodgers LS, Beam MT, Anderson JM, and Fanning AS, “Epithelial barrier assembly requires coordinated activity of multiple domains of the tight junction protein ZO-1,” Journal of Cell Science, vol. 126, no. 7, pp. 1565–1575,2013. [PubMed: 23418357]

[62]. Seebach J, Taha AA, Lenk J, Lindemann N, Jiang X, Brinkmann K, Bogdan S, and Schnittler HJ, “The CellBorderTracker, a novel tool to quantitatively analyze spatiotemporal endothelial junction dynamics at the subcellular level,” Histochem Cell Biol, vol. 144, no. 6, pp. 517–32, 12, 2015. [PubMed: 26275669]

[63]. Rabiet M-J, Plantier J-L, Rival Y, Genoux Y, Lampugnani M-G, and Dejana E, “Thrombin-Induced Increase in Endothelial Permeability Is Associated With Changes in Cell-to-Cell Junction Organization,” Arteriosclerosis, Thrombosis, and Vascular Biology, vol. 16, no. 3, pp. 488–496, 1996.

[64]. Lampugnani MG, Corada M, Caveda L, Breviario F, Ayalon O, Geiger B, and Dejana E, “The molecular organization of endothelial cell to cell junctions: differential association of plakoglobin, beta-catenin, and alpha-catenin with vascular endothelial cadherin (VE-cadherin),” J Cell Biol, vol. 129, no. 1, pp. 203–17, 4, 1995. [PubMed: 7698986]

[65]. Seebach J, Donnert G, Kronstein R, Werth S, Wojciak-Stothard B, Falzarano D, Mrowietz C, Hell SW, and Schnittler HJ, “Regulation of endothelial barrier function during flow-induced conversion to an arterial phenotype,” Cardiovasc Res, vol. 75, no. 3, pp. 596–607, 8 1, 2007. [PubMed: 17531214]

[66]. Geyer H, Geyer R, Odenthal-Schnittler M, and Schnittler HJ, “Characterization of human vascular endothelial cadherin glycans,” Glycobiology, vol. 9, no. 9, pp. 915–25, 9, 1999. [PubMed: 10460833]

[67]. Seebach J, Cao J, and Schnittler HJ, “Quantitative dynamics of VE-cadherin at endothelial cell junctions at a glance: basic requirements and current concepts,” Discoveries, vol. 4, no. 3, pp. e63, 2016. [PubMed: 32309583]

[68]. Ferreri DM, Minnear FL, Yin T, Kowalczyk AP, and Vincent PA, “N-cadherin levels in endothelial cells are regulated by monolayer maturity and p120 availability,” Cell communication & adhesion, vol. 15, no. 4, pp. 333–349, 2008. [PubMed: 18979298]

[69]. Lampugnani MG, Corada M, Andriopoulou P, Esser S, Risau W, and Dejana E, “Cell confluence regulates tyrosine phosphorylation of adherens junction components in endothelial cells,” Journal of Cell Science, vol. 110, no. 17, pp. 2065–2077, 1997. [PubMed: 9378757]

[70]. Abu Taha A, Taha M, Seebach J, and Schnittler H-J, “ARP2/3-mediated junction-associated lamellipodia control VE-cadherin-based cell junction dynamics and maintain monolayer integrity,” Molecular biology of the cell, vol. 25, no. 2, pp. 245–256, 2014. [PubMed: 24227887]

[71]. Gavard J, “Endothelial permeability and VE-cadherin: a wacky comradeship,” Cell adhesion & migration, vol. 8, no. 2, pp. 158–164, 2014. [PubMed: 25422846]

[72]. Biemans EALM, Jäkel L, de Waal RMW, Kuiperij HB, and Verbeek MM, “Limitations of the hCMEC/D3 cell line as a model for Aβ clearance by the human blood-brain barrier,” Journal of neuroscience research, vol. 95, no. 7, pp. 1513–1522, 2017. [PubMed: 27726164]

[73]. Thomas A, Wang S, Sohrabi S, Orr C, He R, Shi W, and Liu Y, “Characterization of vascular permeability using a biomimetic microfluidic blood vessel model,” Biomicrofluidics, vol. 11, no. 2, pp. 024102–024102, 2017. [PubMed: 28344727]

[74]. Perrot CY, Sawada J, and Komatsu M, “Prolonged activation of cAMP signaling leads to endothelial barrier disruption via transcriptional repression of RRAS,” Faseb j, pp. fj201700818RRR, 5 18, 2018.

[75]. Bulbake U, Doppalapudi S, Kommineni N, and Khan W, “Liposomal Formulations in Clinical Use: An Updated Review,” Pharmaceutics, vol. 9, no. 2, pp. 12, 2017.

[76]. Gabizon A, Shmeeda H, and Barenholz Y, “Pharmacokinetics of pegylated liposomal Doxorubicin: review of animal and human studies,” Clin Pharmacokinet, vol. 42, no. 5, pp. 419–36, 2003. [PubMed: 12739982]

[77]. Dai T, Jiang K, and Lu W, “Liposomes and lipid disks traverse the BBB and BBTB as intact forms as revealed by two-step Förster resonance energy transfer imaging,” Acta pharmaceutica Sinica. B, vol. 8, no. 2, pp. 261–271,2018. [PubMed: 29719787]

[78]. Huwyler J, Wu D, and Pardridge WM, “Brain drug delivery of small molecules using immunoliposomes,” Proceedings of the National Academy of Sciences of the United States of America, vol. 93, no. 24, pp. 14164–14169, 1996. [PubMed: 8943078]

[79]. Johnsen KB, Burkhart A, Melander F, Kempen PJ, Vejlebo JB, Siupka P, Nielsen MS, Andresen TL, and Moos T, “Targeting transferrin receptors at the blood-brain barrier improves the uptake of immunoliposomes and subsequent cargo transport into the brain parenchyma,” Scientific Reports, vol. 7, no. 1, pp. 10396, 2017/09/04, 2017. [PubMed: 28871203]

[80]. Kang Y-S, Jung H-J, Oh J-S, and Song D-Y, “Use of PEGylated Immunoliposomes to Deliver Dopamine Across the Blood-Brain Barrier in a Rat Model of Parkinson’s Disease,” CNS Neuroscience & Therapeutics, vol. 22, no. 10, pp. 817–823, 2016. [PubMed: 27350533]

[81]. Schnyder A, Krahenbuhl S, Drewe J, and Huwyler J, “Targeting of daunomycin using biotinylated immunoliposomes: pharmacokinetics, tissue distribution and in vitro pharmacological effects,” J Drug Target, vol. 13, no. 5, pp. 325–35, 6, 2005. [PubMed: 16199376]

[82]. Afergan E, Epstein H, Dahan R, Koroukhov N, Rohekar K, Danenberg HD, and Golomb G, “Delivery of serotonin to the brain by monocytes following phagocytosis of liposomes,” Journal of Controlled Release, vol. 132, no. 2, pp. 84–90, 2008/12/08/, 2008. [PubMed: 18805446]

[83]. Lélu S, Afadzi M, Berg S, Åslund AKO, Torp SH, Sattler W, and Davies C. d. L., “Primary Porcine Brain Endothelial Cells as In Vitro Model to Study Effects of Ultrasound and Microbubbles on Blood-Brain Barrier Function,” IEEE Transactions on Ultrasonics, Ferroelectrics, and Frequency Control, vol. 64, no. 1, pp. 281–290, 2017.

[84]. Fan L, Liu Y, Ying H, Xue Y, Zhang Z, Wang P, Liu L, and Zhang H, “Increasing of Blood-tumor Barrier Permeability through Paracellular Pathway by Low-frequency Ultrasound Irradiation In Vitro,” Journal of Molecular Neuroscience, vol. 43, no. 3, pp. 541–548, 2011/03/01,2011. [PubMed: 21104456]

[85]. Sherriff J, Tamangani J, Senthil L, Cruickshank G, Spooner D, Jones B, Brookes C, and Sanghera P, “Patterns of relapse in glioblastoma multiforme following concomitant chemoradiotherapy with temozolomide,” The British Journal of Radiology, vol. 86, no. 1022, pp. 20120414, 2013. [PubMed: 23385995]

[86]. Wallner KE, Galicich JH, Krol G, Arbit E, and Malkin MG, “Patterns of failure following treatment for glioblastoma multiforme and anaplastic astrocytoma,” Int J Radiat Oncol Biol Phys, vol. 16, no. 6, pp. 1405–9, 6, 1989. [PubMed: 2542195]

[87]. Inglut CT, Gaitan B, Najafali D, Lopez IA, Connolly NP, Orsila S, Perttilä R, Woodworth GF, Chen Y, and Huang H-C, “Predictors and Limitations of the Penetration Depth of Photodynamic Effects in the Rodent Brain,” Photochemistry and Photobiology, vol. 96, no. 2, pp. 301–309, 23 8 2019, 2019. [PubMed: 31441057]

[88]. Stepp H, and Stummer W, “5-ALA in the management of malignant glioma,” Lasers Surg Med, vol. 50, no. 5, pp. 399–419, 7, 2018. [PubMed: 29737540]

[89]. Stepp H, and Stummer W, “Light can treat inoperable brain tumours,” Nature, vol. 565, no. 7738, pp. 161, 1, 2019.

[90]. Salem U, Kumar VA, Madewell JE, Schomer DF, de Almeida Bastos DC, Zinn PO, Weinberg JS, Rao G, Prabhu SS, and Colen RR, “Neurosurgical applications of MRI guided laser interstitial thermal therapy (LITT),” Cancer Imaging, vol. 19, no. 1, pp. 65, 10 15, 2019. [PubMed: 31615562]

[91]. Ashraf O, Patel NV, Hanft S, and Danish SF, “Laser-Induced Thermal Therapy in Neuro-Oncology: A Review,” World Neurosurg, vol. 112, pp. 166–177, 4, 2018. [PubMed: 29410102]

[92]. Silva D, Sharma M, Juthani R, Meola A, and Barnett GH, “Magnetic Resonance Thermometry and Laser Interstitial Thermal Therapy for Brain Tumors,” Neurosurg Clin N Am, vol. 28, no. 4, pp. 525–533, 10, 2017. [PubMed: 28917281]

[93]. Hadjipanayis CG, and Stummer W, “5-ALA and FDA approval for glioma surgery,” J Neurooncol, vol. 141, no. 3, pp. 479–486, 2, 2019. [PubMed: 30644008]

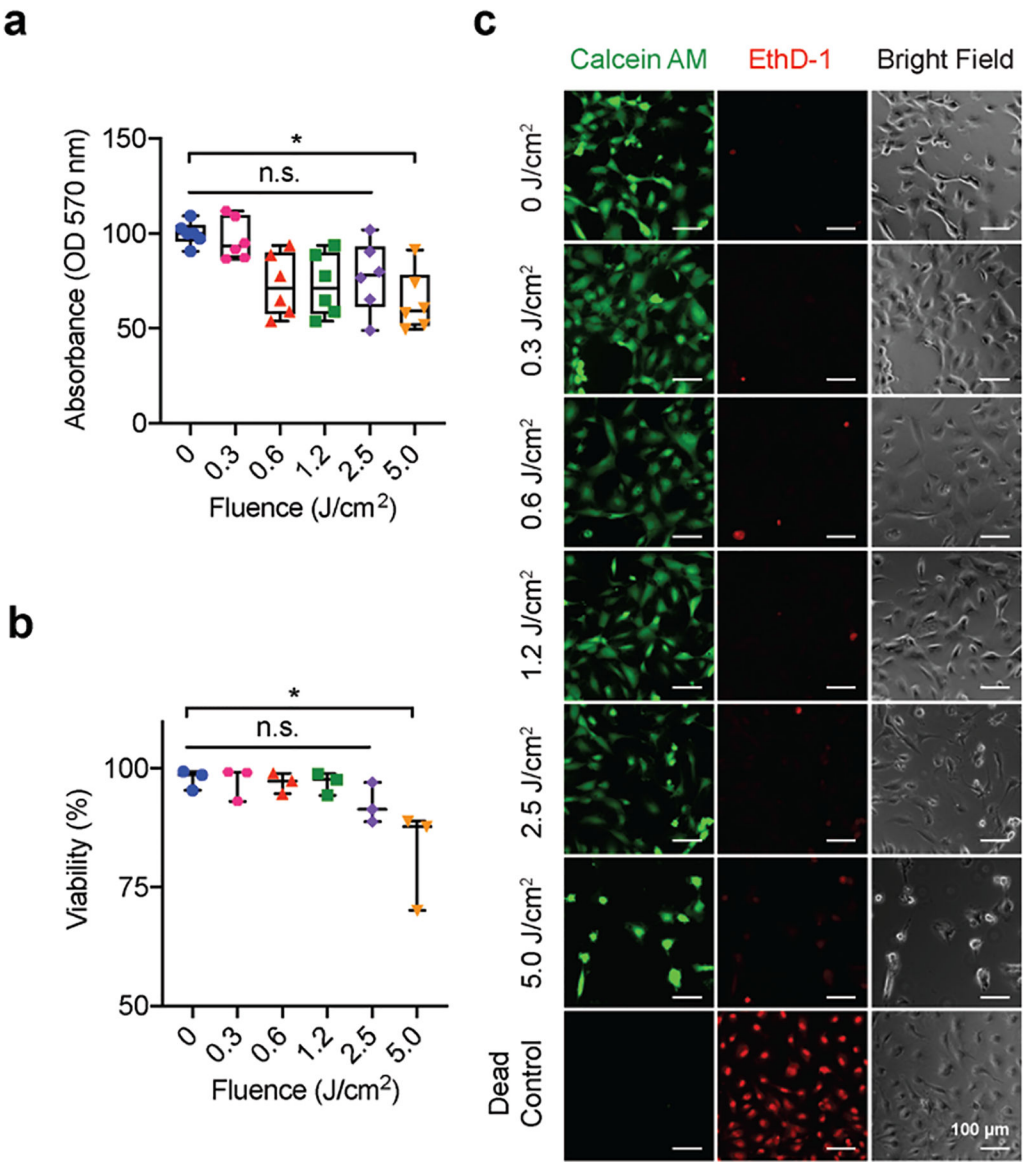


**Fig. 1.**

PDP is sub-cytotoxic to human brain microvascular endothelial cells (HBMECs). HBMECs were incubation with BPD (0.25 µM) for 24 hours followed by light activation (690 nm, 0–5 J/cm$^2$, 6 mW/cm$^2$). The metabolic activity and viability of HBMECs were examined via (a) MTT assay (b) Live/Dead® imaging at 72 hours and 24 hours post-PDP, respectively. Cells incubated with 70% methanol for 30 minutes prior to the addition of Live/Dead® reagents served as the dead control (assay manufacture recommendation), (c) Representative images from the Live/Dead® assay (green channel: Calcein AM, red channel: ethidium homodimer-1, EthD-1) show a confluent monolayer up to a PDP dose of 1.2 J/cm$^2$ (scale bars = 100 µm). Cell viability and metabolic activity were only significantly reduced by the 5.0 J/cm$^2$ PDP dose. For Live/Dead® analysis, a One-Way ANOVA with multiple comparisons was used to calculate significant differences, where n.s. indicates not significant ($p > 0.05$), * $p < 0.05$. N=3, where N equals the number of trials performed. For

MTT analysis, the Kruskal-Wallis test with a Dunn's multiple comparison test was used to calculate significant differences, where n.s. indicates not significant ($p > 0.05$), * $p < 0.05$. N=6, where N equals the number of wells assessed over 3 trials. Box plots show the mean and the likely range of variation. Error bars show the maximum and minimum values.

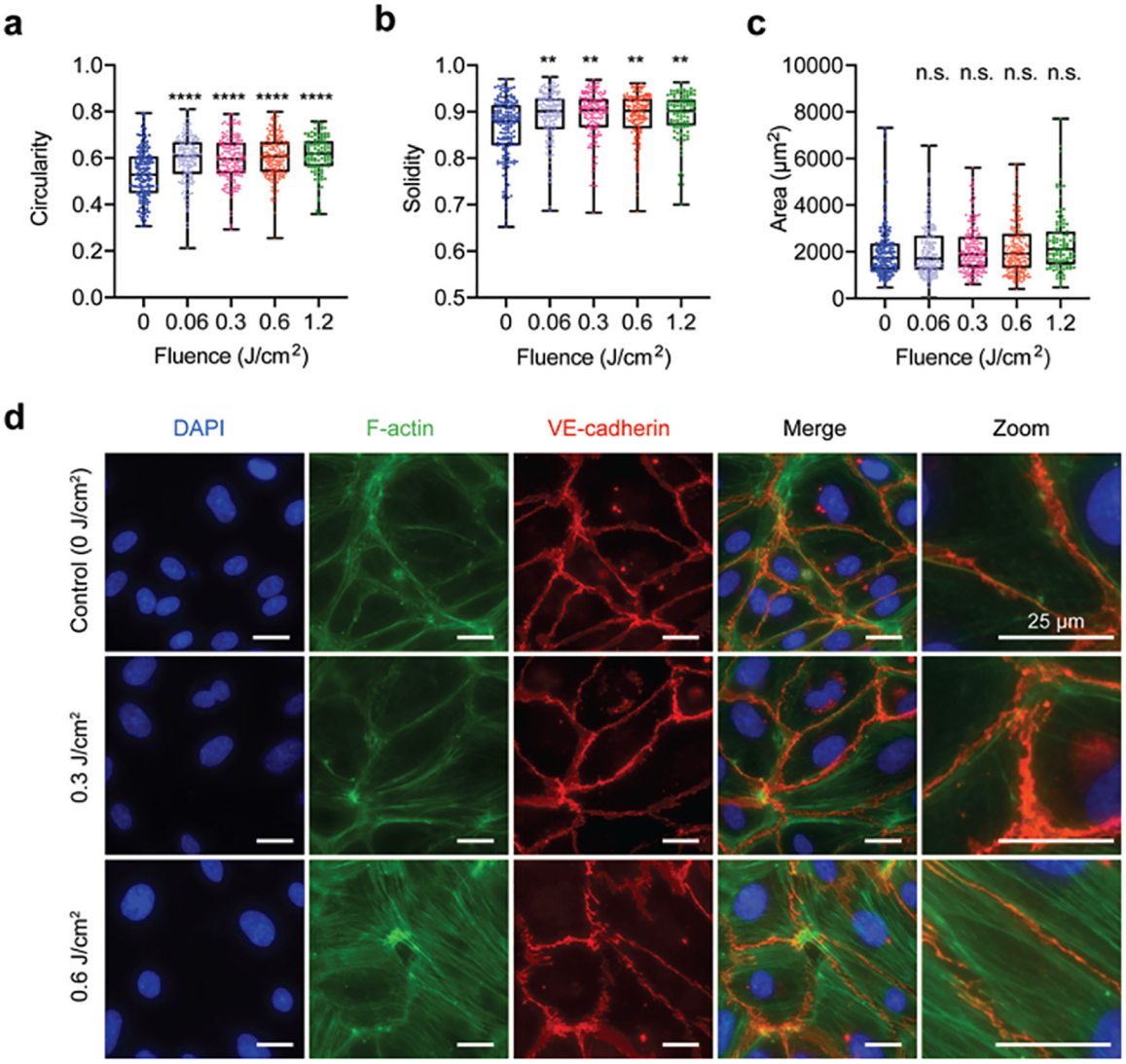


**Fig. 2.**

PDP alters cell morphology and the organization of F-actin. HBMECs were grown to confluency and primed with 690nm red light (0–1.2 J/cm$^2$, 6 mW/cm$^2$). At 90 minutes post priming, cells were fixed and stained for F-actin and VE-cadherin. (a-c) Cell shape factors. All PDP light doses modestly increase HBMEC (a) circularity and (b) solidity. (c) PDP had no impact on HBMEC area. (d) Representative fluorescence images of F-actin (green) organization. VE-cadherin (red) staining is used to show the cell edge. PDP light doses ≥ 0.6 J/cm$^2$ resulted in the rearrangement of F-actin from cortical bands near the cell boundary to stress fibers throughout the cell. All scale bars are 25 μm. The Kruskal-Wallis test with a Dunn's multiple comparison test was used to calculate significant differences, where n.s. indicates not significant ($p > 0.05$), ** $p < 0.01$, *** $p < 0.001$, and **** $p < 0.0001$. The significance between the experiment group and the control is presented. $N > 105$, where N is the number of cells, from 3 different trials. Box plots show the mean and the likely range of variation. Error bars show the maximum and minimum values.

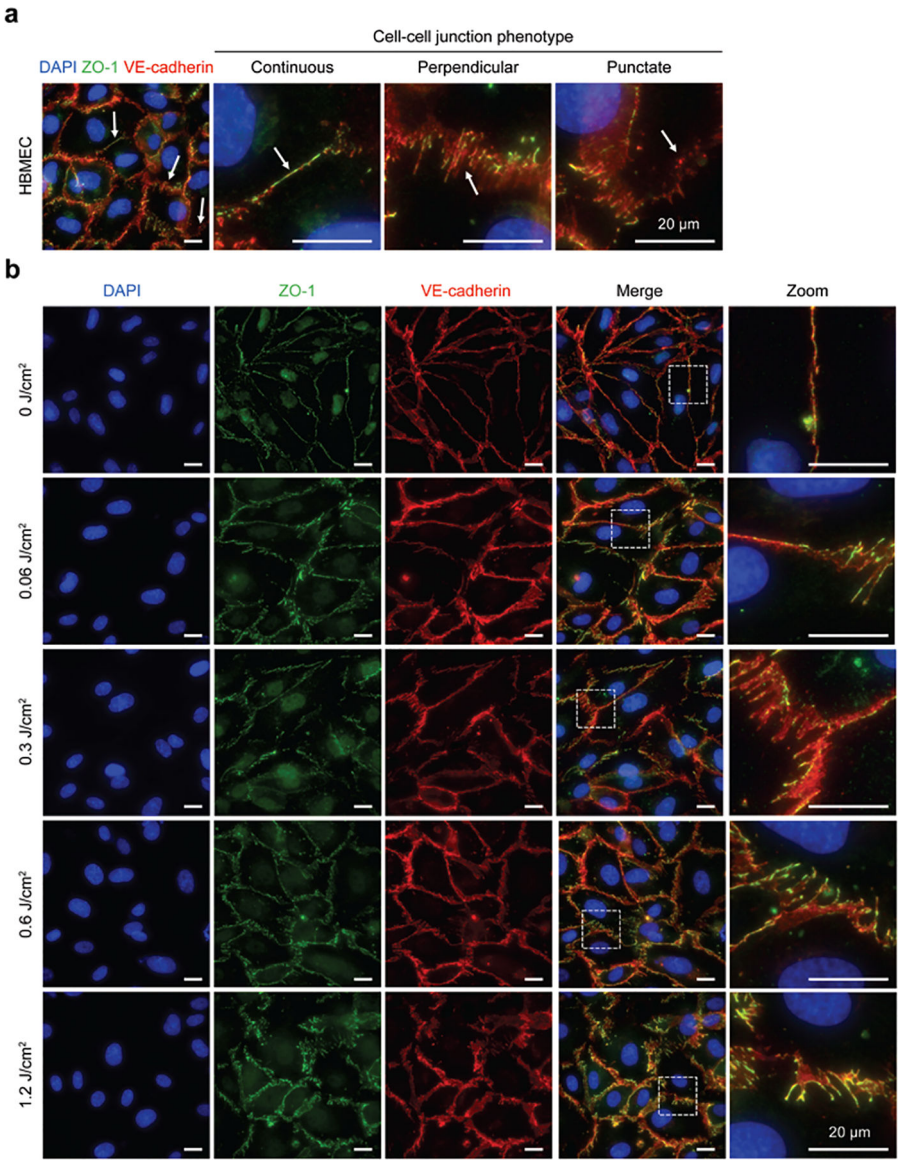


**Fig. 3.**

PDP modulates endothelial cell-cell junction phenotype. At 90 minutes post-priming, cells were fixed, stained, and imaged, (a) Representative fluorescence image of PDP modulated HBMEC with stained nuclei (blue), ZO-1 (green), and VE-cadherin (red). White arrows show regions of different cell-cell junction phenotypes: continuous linear junctions, perpendicular junctions, and dotted punctate junctions. (b) Representative fluorescence images of non-treated cells (0 J/cm$^2$) and photodynamic primed cells (0.06–1.2 J/cm$^2$). PDP generates immature HBMEC monolayers by decreasing linear continuous junctions and increasing perpendicular junctions, in a light dose-dependent manner. All scale bars are 20 μm.

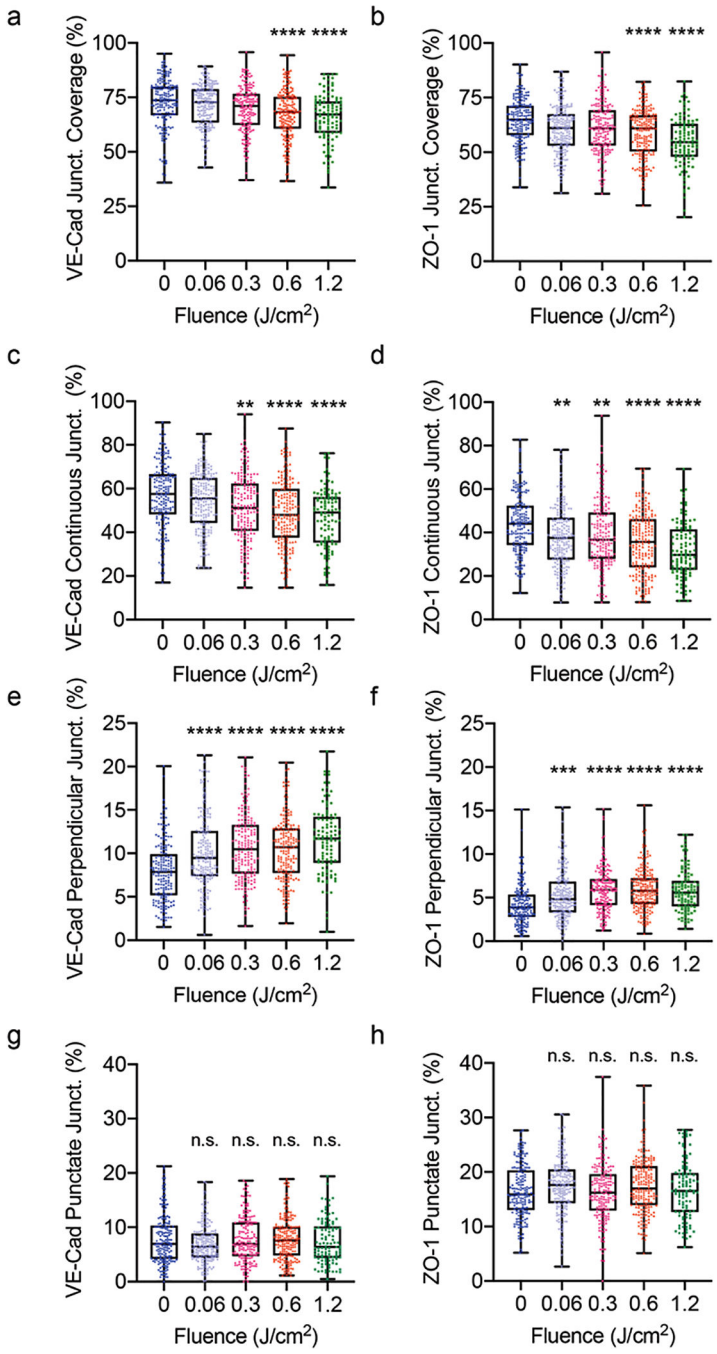


**Fig. 4.**

Quantitative analysis of junction phenotype. At 90 minutes post-priming (0–1.2 J/cm$^2$, 6 mW/cm$^2$), cells were fixed, stained, and analyzed with the Junction Analyzer Program. (a, b) The percent of the cell edge that is covered by a junction, for VE-cadherin and ZO-1, respectively. Edge presentation of continuous (c, d), perpendicular (e, f), and punctate (g, h) junctions for VE-cadherin and ZO-1, respectively. PDP resulted in a light dose-dependent decrease in mature junctions and an increase in unstable junctions. The Kruskal-Wallis test with a Dunn's multiple comparison test was used to calculate significant differences, where

n.s. indicates not significant ($p > 0.05$), ** $p < 0.01$, *** $p < 0.001$, and **** $p < 0.0001$. Please note that not all figure Y- axes are the same magnitude (a-d, 0–100%, e-f, 0–25%, g-h, 0–40%). The significance between the experiment group and the control is presented. $N > 105$, where N is the number of cells assessed over 3 trials. Box plots show the mean and the likely range of variation. Error bars show the maximum and minimum values.

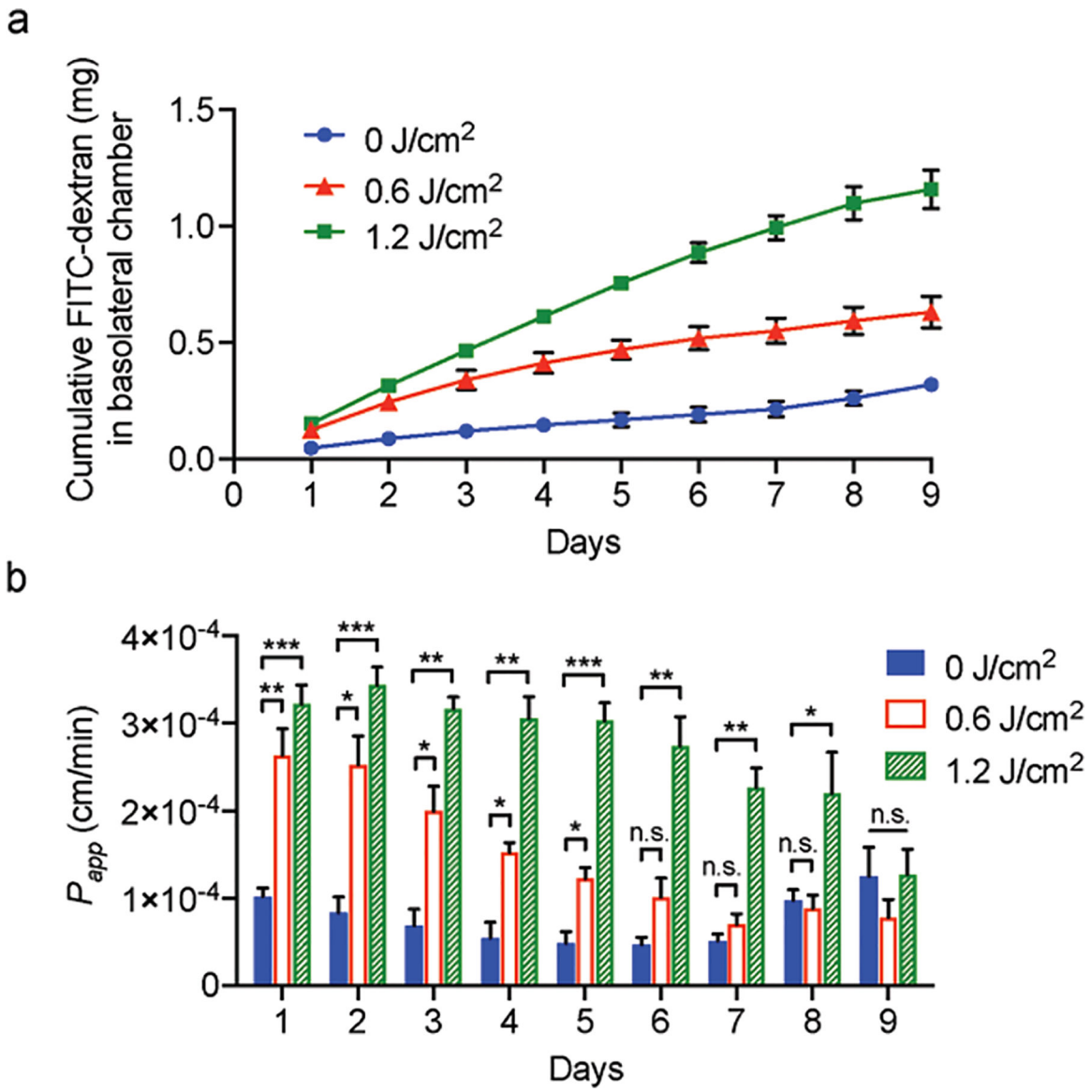


**Fig. 5.**

PDP improves HBMEC monolayer permeability to FITC-dextran. (a) Cumulative FITC-dextran that traversed the HBMEC transwell model. Over 9 consecutive days, PDP (0.6–1.2 J/cm$^2$, 6 mW/cm$^2$) resulted in 2.6–4-fold more FITC-dextran crossing into the bottom transwell chamber. (b) Apparent permeability coefficient, Papp. PDP temporarily and reversibly induced a relatively high degree of permeability in HBMECs. By day 6 and 9, the integrity of the monolayers recovered. A two-way ANOVA with multiple comparisons was used to determine significance, where n.s. indicates not significant ($p > 0.05$), * $p < 0.05$, ** $p < 0.01$, *** $p < 0.001$, and **** $p < 0.0001$. The significance between the experiment group and the control is presented. $N \geq 5$, where N is the number of inserts measured over 3 trials. Error bars show standard error of the mean.

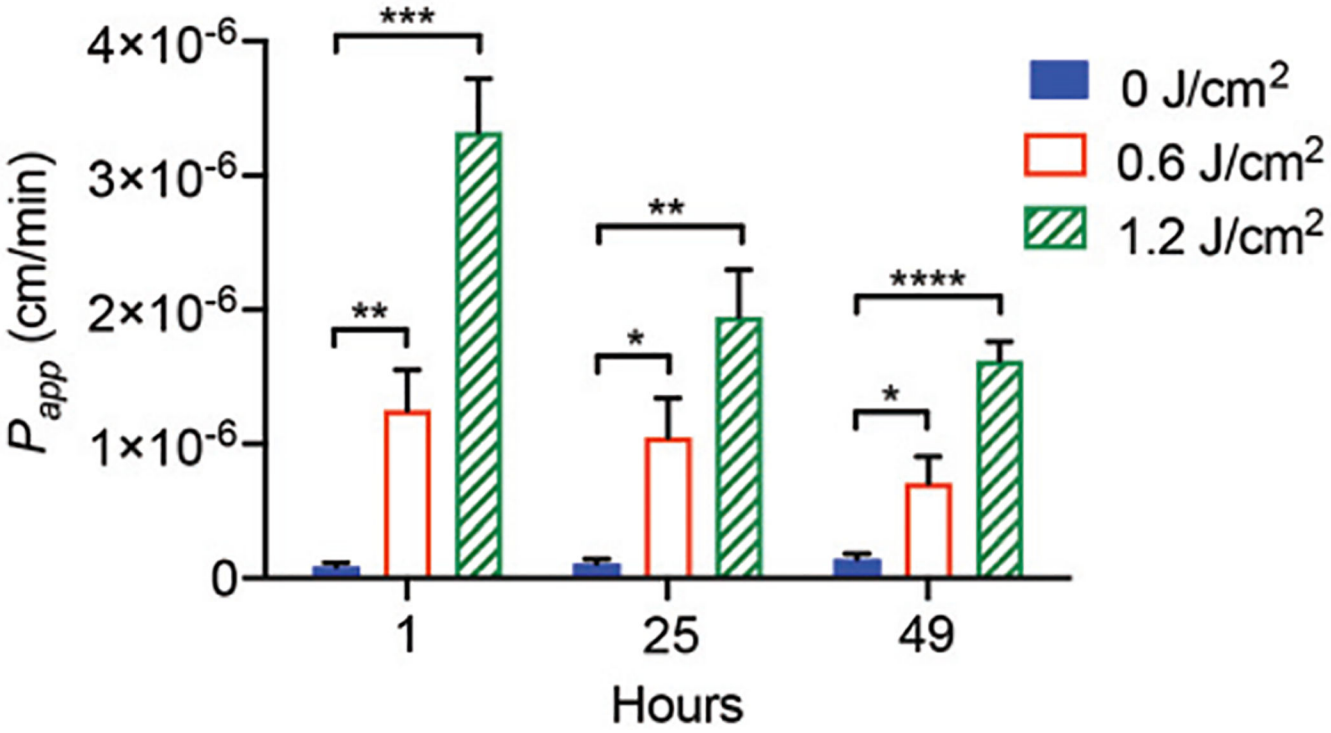


**Fig. 6.**

PDP improves HBMEC monolayer permeability to rhodamine-nanoliposomes. Priming (0.6–1.2 J/cm$^2$, 6 mW/cm$^2$) the transwells resulted in the apparent permeability coefficient, $P_{app}$, of the HBMECs to increase by as much as 38.5-fold, allowing rhodamine-nanoliposomes to diffuse into the basolateral chamber. A two-way ANOVA with multiple comparisons was used to determine significance, where n.s. indicates not significant ($p > 0.05$), * $p < 0.05$, ** $p < 0.01$, *** $p < 0.001$, and **** $p < 0.0001$. The significance between the experiment group and the control is presented. $N \geq 5$, where N is the number of inserts measured over 3 trials. Error bars show standard error of the mean.